DOI: 10.1002/cmdc.200800196

Pyridylalanine-Containing Hydroxamic Acids as Selective HDAC6 Inhibitors

Stefan Schäfer,[a] Laura Saunders,[b] Sonja Schlimme,[c] Vassil Valkov,[a] Julia M. Wagner,[a] Felix Kratz,[d] Wolfgang Sippl,[c] Eric Verdin,[b] and Manfred Jung*[a]

We synthesized hydroxamic acids with a pyridylalanine substructure and identified them as selective inhibitors of human recombinant HDAC6. The in vitro selectivity was up to 25-fold for HDAC6 over HDAC1 and was confirmed by Western blotting to assess tubulin versus histone acetylation in cancer cells. Docking studies with an HDAC6 homology model suggested that the hydrophobic cap group of the inhibitors interacts with aromatic residues that form a sub-pocket near the entrance of the substrate binding channel. The HDAC6-selective compounds have less cytotoxicity toward cancer cells than do pan-HDAC inhibitors. The synergistic antiproliferative activity we showed with the proteasome inhibitor bortezomib suggests the potential for combination anticancer therapy with less general toxicity.

Introduction

The reversible acetylation of histones and other proteins has emerged over the last 10 years as an important mechanism for cell proliferation and has been identified as a valuable target for anticancer drug design. Acetylation is executed and maintained by the histone acetyltransferases and is reversed by their counterparts, the histone deacetylases (HDACs). The first HDAC inhibitor has been approved for therapeutic use, and many additional clinical studies are underway.[1,2–5]

HDACs are zinc-dependent amidohydrolases, and 11 human subtypes are known.[6] Among the dozens of nonhistone substrates of HDACs, tubulin has attracted a lot of attention because it is a bona fide target for established anticancer drugs, such as the vinca-alkaloids and their derivatives and taxanes. Tubulin is deacetylated by a single zinc-dependent HDAC subtype, HDAC6,[7–9] and deacetylated by the NAD^+-dependent histone deacetylase Sirt2.[10] Inhibitors of HDAC6,[11] but also unselective HDAC inhibitors,[12] synergize with the proteasome inhibitor bortezomib (Velcade), which makes HDAC6 an interesting target for inhibitor development. Reports thus far on HDAC6-selective inhibitors are limited[8,13,14] relative to unselective or class I selective inhibitors.[15] Following up our initial reports on phenylalanine-derived hydroxamic acids as HDAC inhibitors,[16,17] we synthesized HDAC6-selective inhibitors with a bromophenylalanine or biarylalanine structure **1** that show selectivity up to 11-fold for HDAC6 over HDAC1 in vitro (see Figure 1).

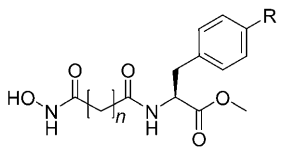

1 $n = 6, 7$
R = –Br, –aryl

Figure 1. Biarylalanine HDAC inhibitors **1**.

Taking the phenylalanine compounds as lead structures, we sought to further modify the amino acid component of the selective inhibitors, and we report herein the synthesis and biological testing of analogues that contain a pyridylalanine element. An initial compound **5d** from that series displayed HDAC6 selectivity.[18] This study showed a difference in the biological effects of an siRNA-mediated knockdown of HDAC6 and competitive inhibition of the enzyme. The major difference was that the protein is still expressed during enzymatic inhibition and thus may still exert signaling effects through protein–protein interactions that go beyond its catalytic activity. The HDAC6-selective inhibitors led to a growth arrest of SKBR3 cancer cells that overexpress the ERBB2 oncogene. Similar to pan-HDAC inhibitors, they induce decay of ERBB2 transcripts, but they do not affect ERBB2-dependent transcription. Conversely, HDAC6 knockdown does not induce ERBB2 transcript decay.

[a] *Dr. S. Schäfer, Dr. V. Valkov, J. M. Wagner, Prof. Dr. M. Jung*
Institute of Pharmaceutical Sciences
Albert-Ludwigs-Universität Freiburg
Albertstr. 25, 79104 Freiburg (Germany)
Fax: (+49) 761-203-6321
E-mail: manfred.jung@pharmazie.uni-freiburg.de

[b] *Dr. L. Saunders, Prof. Dr. E. Verdin*
Gladstone Institute of Virology and Immunology
University of California, San Francisco
1650 Owens Street, San Francisco, CA 94158 (USA)

[c] *Dr. S. Schlimme, Prof. Dr. W. Sippl*
Institute of Pharmacy
Martin-Luther-Universität Halle-Wittenberg
Wolfgang-Langenbeckstr. 4, 06120 Halle (Saale) (Germany)

[d] *Dr. F. Kratz*
Tumor Biology Center, Breisacher Str. 117, 79106 Freiburg (Germany)

Supporting information for this article is available on the WWW under http://dx.doi.org/10.1002/cmdc.200800196: Western blots for histone and tubulin hyperacetylation, figures of the binding mode of enantiomers, and spectral data of inhibitors and intermediates.

In this study, to obtain structure–activity relationships concerning HDAC inhibition, we synthesized a small series of pyridylalanines. As before, we studied the influence of the spacer length and also analyzed the relevance of the stereochemistry. For the investigation of subtype selectivity, HDAC1 and HDAC6 were used in in vitro assays. To elucidate the potential binding mode of the inhibitors, docking studies were performed using established homology models of HDAC1 and HDAC6. The selectivities observed in vitro were validated by comparing histone and tubulin hyperacetylation in cancer cells. The antiproliferative properties of the new inhibitors were studied on MCF7 breast cancer cells and synergy studies with bortezomib were performed, and revealed synergy at nontoxic concentrations of bortezomib.

Table 1. HDAC-inhibitory activity of **5a–g**.

				$IC_{50} \pm SE$ [μM]				
			Enzyme:	Rat liver HDAC			HDAC1	HDAC6
				Subtype selectivity of substrate				
Compd	*n*	Config	-R:	None	HDAC1	HDAC6	None	None
5a	6	*S*	-H	1.52 ± 0.22	33.88 ± 3.98	6.12 ± 0.15	100.46 ± 12.33	3.97 ± 0.74
5b	6	*R*	-H	2.16 ± 0.37	20.46 ± 1.92	5.97 ± 0.15	109.90 ± 13.61	8.48 ± 1.81
5c	7	*S*	-H	1.38 ± 0.09	4.11 ± 0.39	1.58 ± 0.10	67.30 ± 6.09	4.06 ± 1.77
5d	7	*R*	-H	1.55 ± 0.16	11.38 ± 1.60	1.64 ± 0.20	82.60 ± 4.96[a]	4.01 ± 1.61[a]
5e	8	*S*	-H	1.38 ± 0.15	12.08 ± 2.86	2.67 ± 0.42	54.70 ± 7.39	6.00 ± 0.89
5f	6	*R,S*	$-CH_3$	4.49 ± 0.34	20.00 ± 3.38	6.70 ± 0.27	75.16 ± 15.42	6.27 ± 1.43
5g	7	*R,S*	$-CH_3$	1.02 ± 0.15	12.22 ± 3.27	2.17 ± 0.24	73.45 ± 2.19	8.33 ± 0.30

[a] Data are from reference [18].

Results and Discussion

Chemistry

The synthesis of the inhibitors was carried out starting with the protected hydroxamates **2** and pyridylalanine methyl esters **3**, in analogy to previous syntheses from our research group[16,17] (see Scheme 1). The hydroxamic acids **5** were released from the *O*-benzyl precursors **4** by hydrogenation.

Enzyme inhibition

The inhibitors **5a–g** were tested in our homogeneous assay with purified rat liver extract as the source of HDAC activity and a small-molecule substrate. All compounds showed inhibition in the low-micromolar range (Table 1). Next, all inhibitors were assayed for the inhibition of HDAC activity with immunoprecipitated FLAG–HDAC1 and FLAG–HDAC6 as reported.[19]

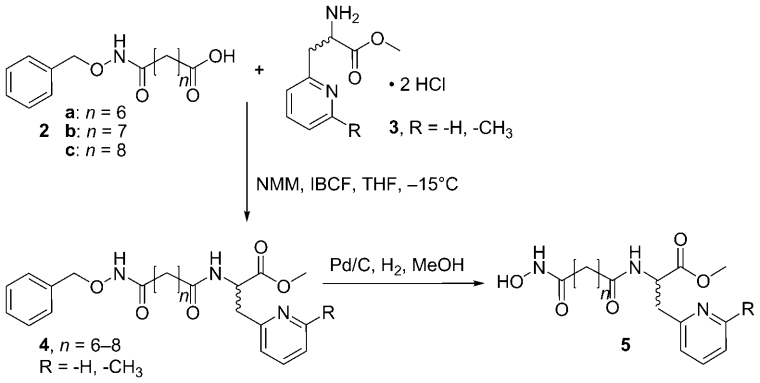

Scheme 1. Synthesis of pyridylalanine-containing HDAC inhibitors. Substituents for **4** and **5**, see Table 1.

We also compared the IC_{50} values obtained with the isolated subtypes with those obtained with subtype-selective substrates[20] and a mixture of subtypes (rat liver extract) (Table 1 and Table 2).

Table 2. Selectivity indices and cytotoxicity.

Compd	Substrates[a] HDAC1/HDAC6	Subtypes[b] HDAC1/HDAC6	GI_{50} [μM][c]
5a	5.54	25.3	104
5b	3.43	13.0	95
5c	2.60	16.6	85
5d	6.94	20.6	73
5e	4.52	9.12	48
5f	2.99	12.0	92
5g	5.63	8.82	42

[a] The predicted selectivities are determined by dividing the IC_{50} values obtained with rat liver HDAC and the subtype-selective substrates (HDAC1/HDAC6). [b] The measured selectivities are determined by dividing the IC_{50} values obtained with immunoprecipitated subtypes and a nonselective substrate (HDAC1/HDAC6). [c] Cytotoxicity is measured as discussed in the Experimental Section (MCF-7 cell line).

The compounds were all predicted to be selective for HDAC6 with the subtype-selective substrates, and indeed for all pyridylalanines, pronounced HDAC6 selectivity was found. For the spacer with six methylene groups, the *S* enantiomer **5a** was more potent toward HDAC6 than the *R* compound **5b.** With the seven-carbon spacer chain, the *R*-configured inhibitor **5d** was more selective than its *S* enantiomer **5c**. An increase to a spacer with eight methylene groups in **5e** led to a loss of selectivity. The inhibitors with the racemic methyl-substituted pyridylalanines **5f–g** also showed decreased selectivity.

To confirm the in vitro selectivity, we compared histone to tubulin hyperacetylation for selected inhibitors **5a** and **5d** in MCF7 breast cancer and HCT116 colon cancer cell lines (see Supporting Information). HDAC1 activity can be correlated to histone deacetylation, and HDAC6 inhibition should lead mainly to tubulin hyperacetylation. For both cell lines

and both compounds, tubulin hyperacetylation was already visible at 1 μM and increased at higher concentrations. In MCF7 cells, **5a** was much more selective for tubulin versus histone hyperacetylation. In HCT116 cells, some histone hyperacetylation was noted for **5a** at 10 μM, but the level of hyperacetylated histone was significantly increased only at 100 μM.

Antiproliferative activities

We next tested the effect of the observed selectivities on cytotoxicity in MCF7 breast cancer cells. HDAC6 is a marker of poor prognosis in estrogen receptor-positive cancers, and the HDAC6 inhibitor tubacin inhibits cell migration in MCF7 cells.[21] As in our previous work on the biarylalanines,[19] we saw a correlation between HDAC6 selectivity and diminished cytotoxicity (Table 2). In general, this could be caused by poor cellular penetration, but we showed that inhibitors **5a** and **5d** induce tubulin hyperacetylation at much lower concentrations.

Because of the known synergism of HDAC inhibitors with the proteasome inhibitor bortezomib, we also investigated the effects of our new HDAC6 inhibitors on the antiproliferative action of bortezomib. We obtained a GI_{50} value for bortezomib of about 20 nM in MCF7 cells. Significant cytotoxicity was only observed at concentrations of 10 nM or greater (see Figure 2A). Cell viability curves were obtained using increasing concentrations of the HDAC6 inhibitors **5d** and **5g** with and without bortezomib (2, 5, and 10 nM) (Figure 2B,C). For **5d**, only at the highest bortezomib concentration was a pronounced leftward shift of the viability curve observed. In the case of **5g**, a clear synergy was seen with 5 nM bortezomib. This con-

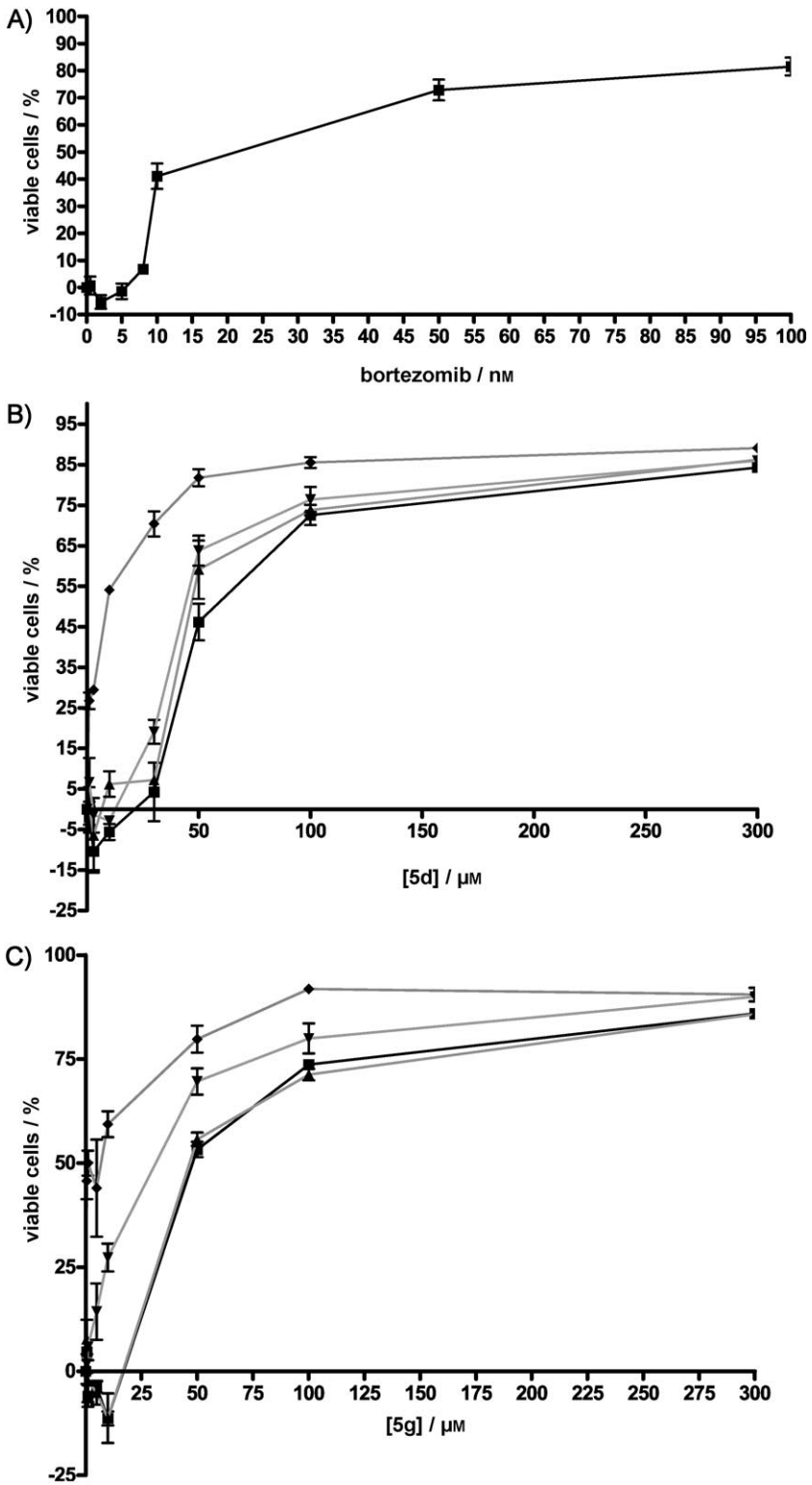

Figure 2. HDAC6 inhibitors and bortezomib in combination show enhanced antiproliferative activity. MCF-7 cells were seeded into 96-well plates; 24 h later, they were treated with HDAC6 inhibitors and bortezomib. Antitumor activity was assessed three days later by MTT assay. A) Antiproliferative effect of bortezomib alone after three days of exposure. B) Viable cells after treatment with **5d** alone, or in combination with bortezomib at 2, 5, and 10 nM for three days. C) Viable cells after treatment with **5g** alone, or in combination with bortezomib at 2, 5, and 10 nM for three days. Cell viability is shown as percentage of control; ■: HDAC inhibitor alone; ▲: HDAC inhibitor + bortezomib (2 nM); ▼: HDAC inhibitor + bortezomib (5 nM); ◆: HDAC inhibitor + bortezomib (10 nM).

centration of the cytotoxic agent is basically ineffective at decreasing cell viability (see Figure 2A). The GI_{50} value of **5g** was reduced from 42 μM to about 30 μM.

An alternative way to look for synergy is to determine the cooperativity index (CI). The Chou–Talalay method[22,23] was used for these combination studies. By looking at the effect each of the two compounds elicits alone and by using a mixture of both agents, we determined if the same effect can be obtained with decreased concentrations of the two agents. The formula for calculation of the CI is given in the Experimental Section. A CI of <1 indicates synergy, and such selectivity was obtained for compound **5g** in a specific dose range (Figure 3).

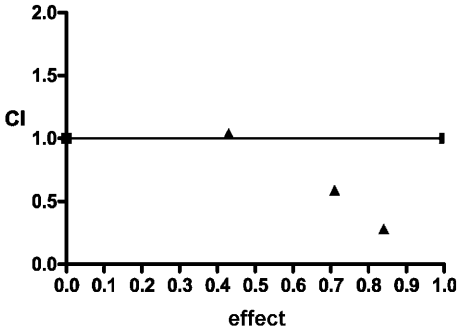

Figure 3. The cooperativity index (CI) was determined as outlined in the Experimental Section. CI <1.0 indicates a synergistic (more than additive) effect. Synergy was observed for a combination of **5g** and bortezomib with CI = 0.59 at 43.2 μM **5g** and 8 nM bortezomib and CI = 0.28 at 54 μM **5g** and 10 nM bortezomib (▲: combination of **5g** and bortezomib).

Analysis of the HDAC binding sites and inhibitor binding modes

The X-ray crystallographic analysis of bacterial HDAC-like proteins (HDLP and FB188 HDAH),[24–27] as well as HDAC7 and HDAC8[26,28] complexes with trichostatin A (TSA) or suberoylanilide hydroxamic acid (SAHA), showed that the HDAC catalytic domain consists of a narrow tube-like pocket spanning a length equivalent to a straight chain of four to six methylene units. Two conserved aromatic residues (Phe152 and Phe208 in FB188 HDAH, Phe152 and Phe208 in HDAC8) located in the tube-like pocket of the HDAC enzymes fix the position of the flexible alkyl spacer of the inhibitors. The catalytic zinc ion, which is buried near the bottom of the active site, is coordinated to His and Asp residues and the hydroxamic acid function of the inhibitors. A similar architecture and interaction pattern are assumed for the related HDAC1 and HDAC6 enzymes.

To better understand the increased HDAC6 activity of the phenylalanine derivatives, compounds **5a**–**g** were docked into homology models of human HDAC1 and HDAC6. Their construction is described elsewhere.[19] The derived HDAC1 and HDAC6 protein models show high structural similarity in the catalytic regions, whereas larger deviations are observed at the entrance region of the binding pocket. In particular, the loop regions forming the entrance of the binding cavity are dissimilar in the different HDAC structures. This model is in accord with other recently published modeling studies on HDAC subtypes.[29,30]

The docking was carried out using the programs GOLD 3.2 and ChemScore as the scoring function. Before docking the novel inhibitors into the HDAC1 and HDAC6 homology models, we first tested the docking program GOLD[31] to determine if it can reproduce the experimentally observed HDAC inhibitor binding modes. We used published X-ray crystallographic structures for HDAH, HDLP, HDAC7, and HDAC8 in complex with different inhibitors from the Protein Data Bank.[32] GOLD with ChemScore could reproduce the inhibitor structures with RMSD values below 2.5 Å.[19]

Next, the inhibitors **5a**–**5g** were docked into the HDAC1 homology model. This showed that the hydroxamic acid interacts with the zinc ion and polar residues (His141 and Tyr303) and that Phe150 and Phe205 sandwich the hydrophobic alkyl chain of the inhibitors. The cap group of **5a**/**5b** and **5c**/**5d** interacts with several aromatic and hydrophobic residues at the entrance of the binding pocket (His28 and Pro29) (Figure 4 shows example docking results for **5a** and **5c**).

The analysis of the docking solutions obtained for the HDAC6 homology model showed that His610 and Tyr782 form hydrogen bonds to the hydroxamic acid of the inhibitors. Phe620 and Phe680 in HDAC6 sandwich the alkyl chain linker between their hydrophobic portions (Figure 5). Larger deviations between HDAC1 and HDAC6 models were observed in the interaction of the bulky cap groups. The HDAC6 model shows a clearly defined hydrophobic binding cavity formed by several aromatic and hydrophobic residues (His499, His500, and Phe566). The docked inhibitors place the hydrophobic cap group in this binding groove (Figure 4A,B). The hydrophobic cavity found in HDAC6 is composed of several aromatic residues, including Phe566 and His560. When looking at the hydrophobic potential of this cavity (Figure 5), the most hydrophobic region detected is near Phe566. Therefore, we suggest that the optimal placement of the hydrophobic aromatic cap group near Phe566 is important for high affinity toward HDAC6. This is to some extent reflected by the high docking scores for compounds that are able to make van der Waals interactions between the cap group and Phe566 (e.g., **5a**, **5b**, **5c**, and **5d**).

The differences in biological activity observed for HDAC1 and HDAC6 were partially clarified by the inspection of the binding mode of the inhibitors. In the case of the HDAC6 model, favorable van der Waals interactions of the hydrophobic cap groups of **5a**/**5b** and **5c**/**5d** with well-defined binding grooves are observed at the entrance of the pocket (His499, His500, and Phe566). Importantly, the aromatic pyridine systems of **5a**/**5b** and **5c**/**5d** show favorable van der Waals interaction with Phe566 (Figure 5A,B). Both *R*- and *S*-configured inhibitor series show a similar binding mode: the aromatic pyridyl substituent interacts with the aromatic groove at the entrance of HDAC6 (see figure 3, Supporting Information). In contrast, the amide group shows a different binding mode and faces in two different directions. These two orientations are also observed in the different SAHA–HDAC7 crystal structures.

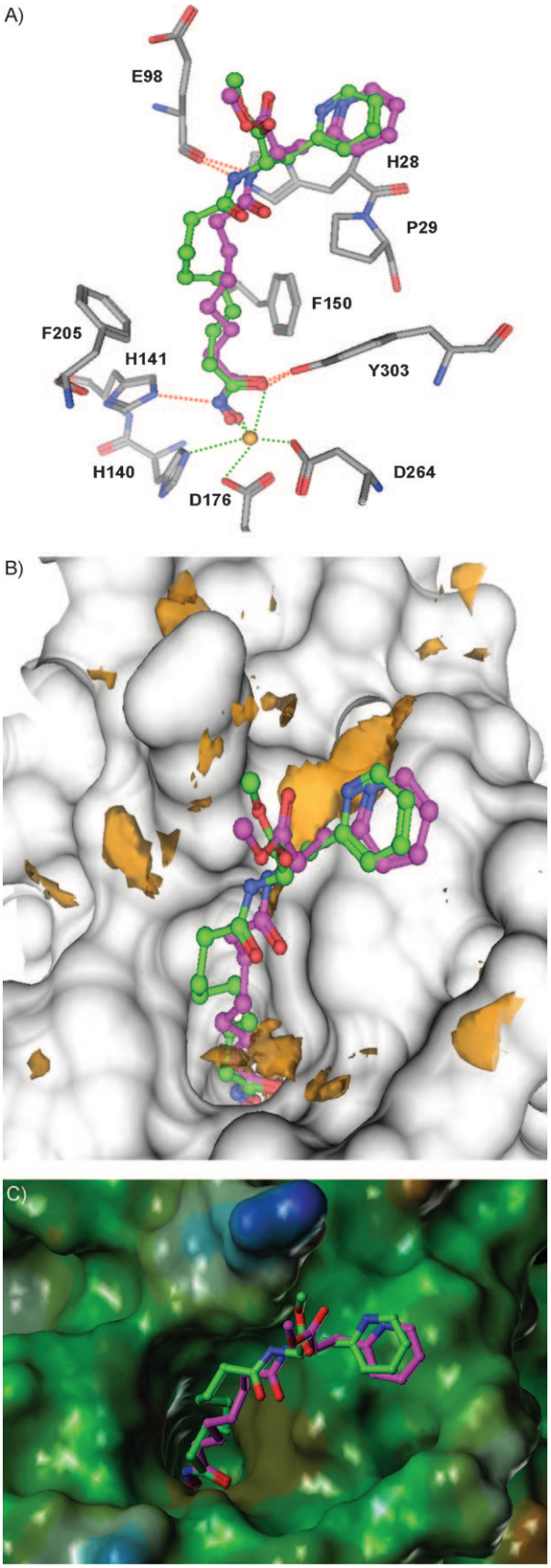

Figure 4. A) GOLD docking solutions for **5a** (magenta) and **5c** (green) at HDAC1. B) The favorable hydrophobic interaction map is shown in orange. C) The surface of the HDAC1 binding pocket is colored according hydrophilicity (brown = hydrophobic, blue = hydrophilic).

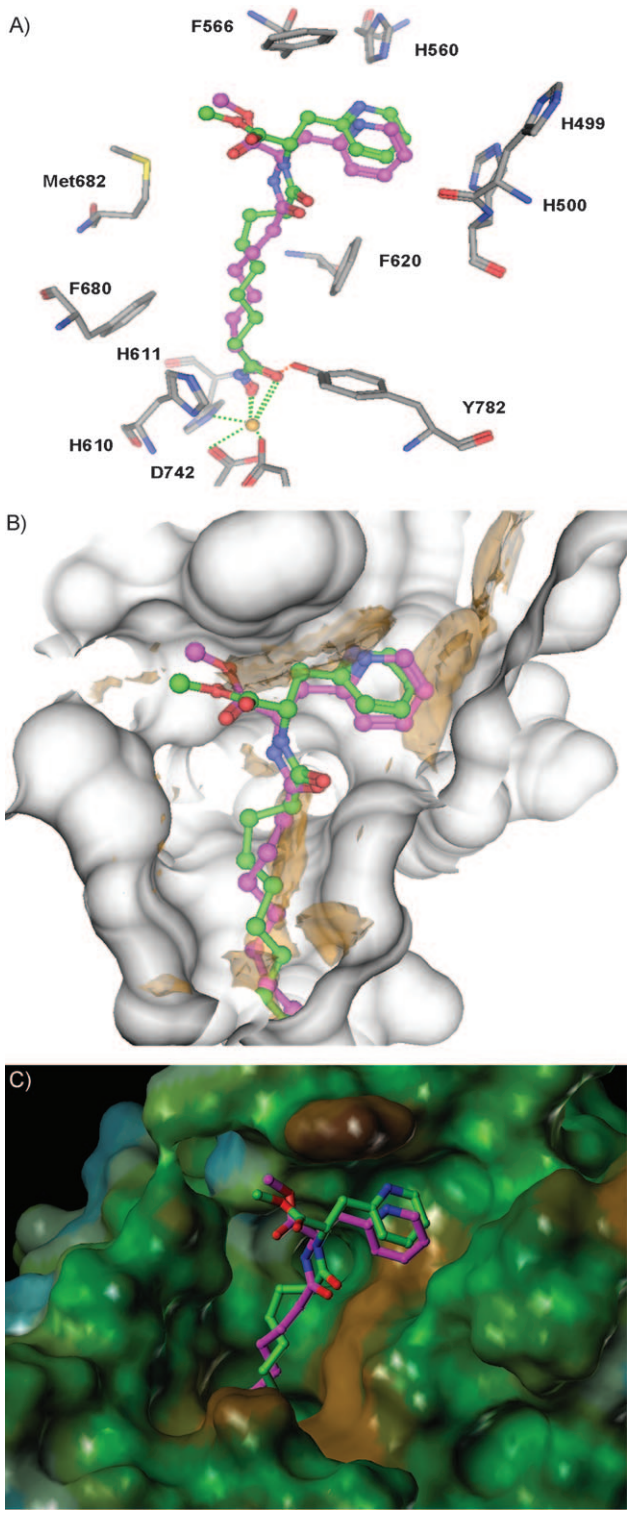

Figure 5. A) GOLD docking solutions for **5a** (magenta) and **5c** (green) at HDAC6. B) The favorable hydrophobic interaction map is shown in orange. C) The surface of the HDAC1 binding pocket is colored according hydrophilicity (brown = hydrophobic, blue = hydrophilic).

In the case of the HDAC1 model, the entrance is less hydrophobic (Figure 4C) and does not show a well-defined groove that accommodates the bulky cap groups. The cap groups are

more solvent exposed, resulting in unfavorable binding characteristics.

The significance of the nonpolar interactions at the entrance of the binding pocket was further analyzed by calculating the nonbonded probability maps for HDAC1 and HDAC6 binding pockets using the MOE software (Chemical Computing Group). The purpose of this knowledge-based approach is to calculate, from the 3D coordinates of the binding site, preferred locations for hydrophobic ligand atoms. As suggested from the docking results, favorable locations for hydrophobic groups are observed for the HDAC6 pocket, whereas the HDAC1 entrance is less hydrophobic (Figure 4B, Figure 5B).

Conclusions

Structure–activity studies on pyridylalanine inhibitors of HDACs have led to the synthesis of selective HDAC6 inhibitors. We gained insight into the structural requirements for the binding of inhibitors to HDAC subtypes by docking the inhibitors into homology models of HDAC1 and HDAC6. In general, the variation of the spacer length showed limited effect in the case of HDAC6 (**5a**, **5c**, and **5e**). The reason for the decreased HDAC1 activities is the diminished ability to bury the hydrophobic cap group of the inhibitors. In HDAC6, the hydrophobic cap groups show a better fit with the aromatic amino acids of the rim of the channel. Regardless of the stereochemistry of the amino acid, good HDAC6 selectivity was obtained. Introduction of an α-methyl group in the pyridyl ring or a spacer length of eight atoms led to a decrease in selectivity over HDAC1. This study again underscores the value of subtype-selective HDAC substrates as tools for the identification of candidate inhibitors for subtype profiling. These HDAC6-selective inhibitors show decreased general toxicity which makes them very promising candidates for combination anticancer therapy (e.g., with the proteasome inhibitor bortezomib).

Experimental Section

General

Melting points are uncorrected and were measured by using an SMP2 melting point apparatus (Stuart Scientific). Elemental analyses were performed with a Vario EL elemental analyzer (Elementar Analysensysteme GmbH, Hanau, Germany). ESI- and APCI-mass spectra were recorded with a LCQ-Advantage mass spectrometer, and EI- and CI-mass spectra with a TSQ700 mass spectrometer (Thermo Electron). NMR spectra were obtained on a Unity 300 spectrometer (300 MHz) by Varian and an Avance DRX 400 spectrometer (400 MHz) by Bruker. Chemical shifts were registered in ppm relative to tetramethylsilane. In some cases, not all signals in the ^{13}C NMR data were resolved (indicated with a footnote). The rat liver HDAC preparation was purified with an Äkta prime chromatography system from Amersham Biosciences. Fluorescence assays were performed on microplate readers (BMG Fluostar Optima and Molecular Devices FlexStation). The fluorescent small-molecule substrates were prepared as reported.[20,33,34] The *O*-benzyl-protected monohydroxamate **2a** was prepared as described.[35] Compounds **2b** and **2c** were synthesized in an analogous fashion from monomethyl nonanedioate and monomethyl decanedioate acid chloride, respectively. The chiral pyridylalanines (R = H) were purchased from Aldrich, the racemic compounds (R = CH_3)[36] were available at our institute. Amino acids were converted into the methyl ester dihydrochlorides by standard procedures with thionyl chloride in anhydrous methanol. Bortezomib was taken from Velcade solutions for injection purchased at the hospital pharmacy of the University of Freiburg. In Velcade, bortezomib is present as a freeze-dried mannitol ester prodrug. The stoichiometry of the complex is not given in the specification, but liberates bortezomib in solution (see prescription information at http://www.velcade.com (accessed November 26, 2008)).

Method A: Amide formation with mixed anhydrides

Carboxylic acid (1 mmol) was dissolved in anhydrous THF (20 mL) and 1 mmol *N*-methylmorpholine (NMM) was added to the solution. The reaction mixture was cooled to −15 °C and stirred for 5 min. Isobutylchloroformate (IBCF, 1 mmol) was added and stirred continuously for another 10 min at −15 °C. Then, 1 mmol of the amine and another 2 mmol of NMM were added, and the mixture was stirred for a further 15 min at −15 °C, and then for 2 h at room temperature. Finally, the mixture was poured into HCl (2 M) and extracted (3×) with EtOAc. The combined organic phases were washed with H_2O (3×), then a solution of $NaHCO_3$ (5%), and H_2O again. After final washing with brine and drying over Na_2SO_4, the product was purified by flash column chromatography with EtOAc as eluent. The product-containing fractions were evaporated, and the residues were crystallized from petroleum ether (80–110 °C). The solid was collected by filtration, and the product was dried under high vacuum.

Method B: Deprotection via hydrogenation

The *O*-benzyl-protected derivatives **4** were dissolved in a few mL MeOH, and 10% (*w*/*w*) Pd/C (10%) was added under N_2. The reaction mixture was then treated with H_2 at atmospheric pressure unless otherwise indicated. After 4 h, the catalyst was filtered off, and the solvent was evaporated. In the case of **5a**, **5b**, and **5e** the crude product was purified by flash chromatography with EtOAc/MeOH (95:5) as eluent. All crude end products were dissolved in a few mL MeOH and then precipitated with Et_2O. After cooling overnight, the solid was collected by filtration, washed with a small volume of Et_2O, and dried under high vacuum. Data for most compounds are given in the Supporting Information. A representative inhibitor with its data is listed below.

(*R*,*S*)-2-(8-Hydroxycarbamoyloctanoylamino)-3-(6-methylpyridin-2-yl)propionic acid methyl ester (**5g**). Method B, **4g** (500 mg, 1.06 mmol), Pd/C (50 mg), MeOH (20 mL). Yield: 206 mg white solid (51%), mp: 107 °C; ^{1}H NMR ([D$_6$]DMSO, 400 MHz): δ = 10.33 (s, 1H, *H*O-NH-CO), 8.67 (s, 1H, HO-N*H*-CO), 8.23 (d, 1H, ^3J = 7.9 Hz, N*H*-CH-CO), 7.59–7.56 (pt (dd), 1H, ^3J = 7.7 Hz, ^3J = 7.7 Hz, 4′-*H*), 7.08 (m, 1H, 3′-*H*), 7.04 (m, 1H, 5′-*H*), 4.69–4.63 (m, 1H, NH-C*H*-CO), 3.60 (s, 3H, COOCH_3), 3.10 (dd, 1H, ^2J = 13.9 Hz, ^3J = 5.4 Hz, CH-CH_2-Ar), 2.98 (dd, 1H, ^2J = 13.9 Hz, ^3J = 9.0 Hz, CH-CH_2-Ar), 2.42 (s, 3H, 6′-CH_3), 2.03 (t, 2H, ^3J = 7.3 Hz, CO-CH_2), 1.92 (t, 2H, ^3J = 7.4 Hz, CO-CH_2), 1.48–1.35 (m, 4H, (CH_2)$_2$), 1.18–1.08 ppm (m, 6H, (CH_2)$_3$); ^{13}C NMR ([D$_6$]DMSO, 100 MHz): δ = 172.73, 172.66, 169.51 (*C*O), 157.64 (2′-*C*), 156.73 (6′-*C*), 137.06 (4′-*C*), 121.50, 121.01 (3′/5′-*C*), 52.39, 52.18 (COO*C*H$_3$, NH-*C*H-CO), 39.24 (CH-*C*H$_2$-Ar), 35.38, 32.66 (CO-*C*H$_2$), 28.89, 28.87, 28.68, 25.53, 25.50 ((*C*H$_2$)$_5$), 24.45 ppm (Ar-*C*H$_3$); MS (APCI +): *m*/*z* = 380 [*M*+H]$^+$; IR (ATR): $\tilde{\nu}$ = 1747 (COOCH$_3$), 1645 cm^{-1} (CO-NH, CO-NH-OH).

Assays

Assays with rat liver extract

Enzyme inhibition was determined using standard reported methods.[19] First, we used a partially purified rat liver extract with a fluorescent substrate (MAL)[33] that is unselective[20] for different subtypes. In a second test series, we used the same enzyme preparation with subtype-selective substrates discovered in our research group[20] to predict subtype selectivity. For HDAC1 prediction *Z*-(propionyl)Lys-AMC was used, and for HDAC6 prediction Boc(Ac)-Lys-(F_3-AMC) was used.

Stock solutions of the inhibitors were prepared at 12 mM in DMSO and further diluted with enzyme buffer (1.4 mM NaH_2PO_4, 18.6 mM Na_2HPO_4, pH 7.9, 0.25 mM EDTA, 10 mM NaCl, 10% (*v*/*v*) glycerol and 10 mM 2-mercaptoethanol) to the desired concentration. Stock solutions of the substrates were prepared in DMSO at 12.6 mM and further diluted with enzyme buffer to a concentration of 126 μM for the assay. Rat liver extract (50 μL) was incubated with 5 μL of the inhibitor dilution and 5 μL of the substrate dilution at 37 °C. Incubation times were 90 min for the unselective substrates and 180 min for the selective substrates. The reaction was stopped by adding 190 μL of freshly prepared stop solution (trichostatin A (TSA) 3.3 μM, borate buffer, pH 9.5, and naphthalene-2,3-dicarboxaldehyde (NDA, 16 mM in MeOH) at a ratio of 5:180:5). Fluorescence was detected at an excitation wavelength of 330 nm and an emission wavelength of 390 nm except for the HDAC6-selective substrate (λ_{ex}: 340 nm, λ_{em}: 430 nm).

Immunoprecipitated FLAG-tagged HDAC1 and HDAC6

FLAG-tagged HDAC1 and HDAC6 were isolated from 293T cell lines overexpressing either HDAC1 or HDAC6 with M2-agarose beads (Sigma) as described.[19] We used the purified subtypes to determine the inhibitory potential with an unselective substrate (called ZMAL)[34] that is suitable for these enzymes.

293T cell lines overexpressing FLAG-tagged HDAC1 and HDAC6 were cultured and lysed. M2-agarose was used at 25 μL mL^{-1} cell lysate. The immunoprecipitated enzymes were washed in enzyme buffer, diluted (1:10) and used as the enzyme source. Bead suspensions of 50 μL were incubated with 5 μL of the inhibitor dilution and 5 μL of the substrate dilution at 37 °C for 180 min. The reaction was stopped by adding 190 μL of freshly prepared stop solution (3.3 μM TSA, borate buffer, pH 9.5 and NDA (16 mM in MeOH) at a ratio of 5:180:5). Fluorescence was measured at an excitation wavelength of 330 nm and an emission wavelength of 390 nm.

Determination of IC_{50} values

The amounts of remaining substrate in the samples were calculated relative to two reference samples equivalent to 0 and 100% enzyme inhibition. For 100% inhibition, we used 50 μL of the enzyme source, 5 μL of a 3.3 μM TSA dilution, and 5 μL of the substrate dilution. For 0% inhibition, we used 50 μL of the enzyme source, 5 μL of enzyme buffer, and 5 μL of the substrate dilution. The IC_{50} values were determined by measuring the enzyme inhibition of a dilution series of the particular inhibitor relative to the standards; this was followed by evaluation with the GraphPad Prism software.

Western blot analysis

MCF-7 human breast adenocarcinoma cells were grown in RPMI-1640 (Gibco Invitrogen) supplemented with 10% fetal bovine serum (FBS; PAA), 1% 2 mM L-glutamine (Gibco Invitrogen) and 1% penicillin–streptomycin (Gibco Invitrogen). HCT116 human colon carcinoma cells were grown in Dulbecco's modified Eagle's medium (DMEM; Mediatech, Herndon, VA, USA) with 10% FBS (Gemini Bio-products, Woodland, CA, USA), 1% penicillin–streptomycin and 2 mM L-glutamine (GIBCO Invitrogen).

Both cell lines were treated with various concentrations of the inhibitors and TSA as a control for 6 h. Cells were lysed in 50 mM Tris-HCl, pH 7.5, 0.5 mM EDTA, 150 mM NaCl, 0.5% NP-40, and 1× complete protease inhibitors (Roche, Penzberg, Germany).

Protein concentrations of lysates of MCF-7 breast adenocarcinoma cells were determined with the BCA™ Protein Assay (Pierce). Protein samples were electrophoresed on 15% SDS–polyacrylamide gels and transferred to an Immobilon-P transfer membrane (Millipore). Membranes were blocked with Roti-Block (Roth) and probed with antibodies against acetylated α-tubulin (Sigma 6-11B-1) 1:2000, anti-α-tubulin (Sigma B-5-1-2) 1:2000, anti-acetylated histone H3 (Upstate 06-599) 1:2000, and anti-acetylated histone H4 (Upstate 06-598) 1:2000.

Protein concentrations of lysates of HCT116 colon carcinoma cells were determined with the D_C Protein Assay (Bio-Rad). Protein samples were electrophoresed on 10% and 15% SDS–polyacrylamide gels and transferred to a nitrocellulose membrane (Bio-Rad). Membranes were blocked with 5% nonfat dry milk in TBS–Tween (10 mM Tris-HCl, pH 7.5, 150 mM NaCl, and 0.1% Tween-20) and probed with anti-acetylated α-tubulin (Sigma 6-11B-1) or anti-α-tubulin (Sigma B-5-1-2) at 1:2000, anti-acetylated histone H3 (Upstate 06-599), and anti-acetylated histone H4 (Upstate 06-866).

Cytotoxicity assays

MCF-7 human breast tumor cells were obtained from Max-Delbrück-Centrum MDC (BerlinBuch) and maintained in RPMI-1640 supplemented with 10% FBS, 1% 2 mM L-glutamine, and 1% penicillin–streptomycin (Invitrogen). The cells were incubated at 37 °C in an atmosphere of 5% CO_2.
Cells were seeded at 5000 per well in 100 μL of growth medium in 96-well tissue culture plates. At 24 h after seeding, diluted compounds or DMSO vehicle control were added to each well and incubated for 72 h at 37 °C. Growth inhibition was determined using the MTT assay. Data were plotted as a percentage of DMSO-treated control against compound concentration using GraphPad Prism 4.0. The 50% growth inhibition (GI_{50}) was calculated as the compound concentration required to decrease cell number by 50% relative to with control.

Analysis of synergism with bortezomib

The Chou–Talalay method[22,23] was used for drug combination studies. It uses the following equation: $CI = (D)1/(Dx)1 + (D)2/(Dx)2$, for which (D)1 and (D)2 are respective doses of drugs 1 and 2 that have the *x* effect used in combination, and (D*x*)1 and (D*x*)2 are the doses of drugs 1 and 2 that have the same effect when used alone. Synergy is present when $CI < 1.0$. The combination is additive when $CI = 1.0$, and is antagonistic when $CI > 1.0$.

Molecular modeling

All calculations were performed on a Pentium 1.8 GHz Linux cluster. The molecular structures of the inhibitors were generated using the MOE modeling package (Chemical Computing Group, Montreal, Canada). The inhibitor structures were energy minimized

using the MMFF94s force field and the conjugate gradient method, until the default derivative convergence criterion of 0.01 kcal mol^{-1} Å^{-1} was met.

Docking of the inhibitors

Homology models were recently generated for HDAC1 and HDAC6, with the COMPOSER module (as part of the Sybyl 7.2 program[37]) and the available X-ray crystal structures of HDLP, HDAC8, and HDAC as templates (for details, see reference [19]). Docking of the known co-crystallized inhibitors, as well as the novel compounds, was carried out using the crystal structures and the HDAC1 and HDCAC6 homology models. Program GOLD 3.2 was used for ligand docking. All torsion angles in each compound were allowed to rotate freely. For each molecule, 30 docking runs were carried out. The resulting solutions were clustered on the basis of the heavy-atom RMSD values (1 Å). We tested several docking setups to reproduce the experimentally derived complexes of HDAC inhibitors. The best agreement between the available crystal structures and docking poses could be derived by applying the ChemScore scoring function within GOLD. A hydrogen bond to the active site histidine (His143 in HDAH, His141 in HDAC1, His216 in HDAC6 CD I, His611 in HDAC6 CD II) was used as docking constraint. This docking setup resulted in good reproduction (RMDS $<$ 2.5 Å) of the experimentally derived structures of SAHA and TSA, which were co-crystallized with several HDACs.[19] The top-ranked poses for each ligand were selected and viewed graphically within the MOE program.

Hydrophobic interaction fields

Interaction possibilities at the binding pockets were analyzed by calculating the contact preferences with the MOE program (Chemical Computing Group). The purpose of this knowledge-based approach is to calculate, from the 3D coordinates of the binding site, preferred locations for hydrophobic ligand atoms. The contact preferences for hydrophobic atoms are calculated on the basis of statistical data derived from experimental 3D structures (Chemical Computing Group). The calculated hydrophobic contact preferences were then viewed superimposed on the crystal structure and homology models using the MOE program.

Acknowledgements

M. Jung and S. Schäfer thank the Hans and Gertie Fischer Foundation for funding, and Sanofi–Aventis for an [i]lab travel award.

Keywords: biological activity · docking · enzymes · histone deacetylases · homology models · hydrolases

[1] R. W. Johnstone, *Nat. Rev. Drug Discovery* **2002**, *1*, 287–299.
[2] S. Minucci, P. G. Pelicci, *Nat. Rev. Cancer* **2006**, *6*, 38–51.
[3] S. Schäfer, M. Jung, *Arch. Pharm.* **2005**, *338*, 347–357.
[4] M. Biel, V. Wascholowski, A. Giannis, *Angew. Chem.* **2005**, *117*, 3248–3280; *Angew. Chem. Int. Ed.* **2005**, *44*, 3186–3216.
[5] T. A. Miller, D. J. Witter, S. Belvedere, *J. Med. Chem.* **2003**, *46*, 5097–5116.
[6] S. G. Gray, T. J. Ekstrom, *Exp. Cell Res.* **2001**, *262*, 75–83.
[7] C. Hubbert, A. Guardiola, R. Shao, Y. Kawaguchi, A. Ito, A. Nixon, M. Yoshida, X. F. Wang, T. P. Yao, *Nature* **2002**, *417*, 455–458.
[8] S. J. Haggarty, K. M. Koeller, J. C. Wong, C. M. Grozinger, S. L. Schreiber, *Proc. Natl. Acad. Sci. USA* **2003**, *100*, 4389–4394.
[9] Y. Zhang, N. Li, C. Caron, G. Matthias, D. Hess, S. Khochbin, P. Matthias, *EMBO J.* **2003**, *22*, 1168–1179.
[10] B. J. North, B. L. Marshall, M. T. Borra, J. M. Denu, E. Verdin, *Mol. Cell* **2003**, *11*, 437–444.
[11] T. Hideshima, J. E. Bradner, J. Wong, D. Chauhan, P. Richardson, S. L. Schreiber, K. C. Anderson, *Proc. Natl. Acad. Sci. USA* **2005**, *102*, 8567–8572.
[12] S. Emanuele, M. Lauricella, D. Carlisi, B. Vassallo, A. D'Anneo, P. Di Fazio, R. Vento, G. Tesoriere, *Apoptosis* **2007**, *12*, 1327–1338.
[13] T. Suzuki, A. Kouketsu, Y. Itoh, S. Hisakawa, S. Maeda, M. Yoshida, H. Nakagawa, N. Miyata, *J. Med. Chem.* **2006**, *49*, 4809–4812.
[14] A. Mai, S. Massa, R. Pezzi, S. Simeoni, D. Rotili, A. Nebbioso, A. Scognamiglio, L. Altucci, P. Loidl, G. Brosch, *J. Med. Chem.* **2005**, *48*, 3344–3353.
[15] M. Paris, M. Porcelloni, M. Binaschi, D. Fattori, *J. Med. Chem.* **2008**, *51*, 1505–1529.
[16] S. Wittich, H. Scherf, C. Xie, G. Brosch, P. Loidl, C. Gerhäuser, M. Jung, *J. Med. Chem.* **2002**, *45*, 3296–3309.
[17] S. Wittich, H. Scherf, C. Xie, B. Heltweg, F. Dequiedt, E. Verdin, C. Gerhäuser, M. Jung, *Anticancer Drugs* **2005**, *16*, 635–643.
[18] G. K. Scott, C. Marx, C. E. Berger, L. R. Saunders, E. Verdin, S. Schäfer, M. Jung, C. C. Benz, *Mol. Cancer Res.* **2008**, *6*, 1250–1258.
[19] S. Schäfer, L. Saunders, E. D. Eliseeva, A. Velena, M. Jung, A. Schwienhorst, A. Strasser, A. Dickmanns, R. Ficner, S. Schlimme, W. Sippl, E. Verdin, M. Jung, *Bioorg. Med. Chem.* **2008**, *16*, 2011–2033.
[20] B. Heltweg, F. Dequiedt, B. L. Marshall, C. Brauch, M. Yoshida, N. Nishino, E. Verdin, M. Jung, *J. Med. Chem.* **2004**, *47*, 5235–5243.
[21] S. Saji, M. Kawakami, S. Hayashi, N. Yoshida, M. Hirose, S. Horiguchi, A. Itoh, N. Funata, S. L. Schreiber, M. Yoshida, M. Toi, *Oncogene* **2005**, *24*, 4531–4539.
[22] T. C. Chou, P. Talalay, *Adv. Enzyme Regul.* **1984**, *22*, 27–55.
[23] T. C. Chou, R. J. Motzer, Y. Tong, G. J. Bosl, *J. Natl. Cancer Inst.* **1994**, *86*, 1517–1524.
[24] M. S. Finnin, J. R. Donigian, A. Cohen, V. M. Richon, R. A. Rifkind, P. A. Marks, R. Breslow, N. P. Pavletich, *Nature* **1999**, *401*, 188–193.
[25] J. R. Somoza, R. J. Skene, B. A. Katz, C. Mol, J. D. Ho, A. J. Jennings, C. Luong, A. Arvai, J. J. Buggy, E. Chi, J. Tang, B. C. Sang, E. Verner, R. Wynands, E. M. Leahy, D. R. Dougan, G. Snell, M. Navre, M. W. Knuth, R. V. Swanson, D. E. McRee, L. W. Tari, *Structure* **2004**, *12*, 1325–1334.
[26] T. K. Nielsen, C. Hildmann, A. Dickmanns, A. Schwienhorst, R. Ficner, *J. Mol. Biol.* **2005**, *354*, 107–120.
[27] T. K. Nielsen, C. Hildmann, D. Riester, D. Wegener, A. Schwienhorst, R. Ficner, *Acta Crystallogr. Sect. F Struct. Biol. Cryst. Commun.* **2007**, *63*, 270–273.
[28] PDB accession code 3C0Y (replaced previous PDB code 2NVR): A. Schuetz, J. R. Min, A. Allali-Hassani, P. Loppnau, N. P. Kwiatkowski, R. Mazitschek, A. M. Edwards, C. H. Arrowsmith, M. Vedadi, A. Bochkarev, A. N. Plotnikov, **2007**, DOI: 10.2210/pdb3c0y/pdb.
[29] G. Estiu, E. Greenberg, C. B. Harrison, N. P. Kwiatkowski, R. Mazitschek, J. E. Bradner, O. Wiest, *J. Med. Chem.* **2008**, *51*, 2896–2906.
[30] P. Siliphaivanh, P. Harrington, D. J. Witter, K. Otte, P. Tempest, S. Kattar, A. M. Kral, J. C. Fleming, S. V. Deshmukh, A. Harsch, P. J. Secrist, T. A. Miller, *Bioorg. Med. Chem. Lett.* **2007**, *17*, 4619–4624.
[31] A. Schuetz, J. Min, A. Allali-Hassani, M. Schapira, M. Shuen, P. Loppnau, R. Mazitschek, N. P. Kwiatkowski, T. A. Lewis, R. L. Maglathin, T. H. McLean, A. Bochkarev, A. N. Plotnikov, M. Vedadi, C. H. Arrowsmith, *J. Biol. Chem.* **2008**, *283*, 11 355–11 363.
[32] H. M. Berman, J. Westbrook, Z. Feng, G. Gilliland, T. N. Bhat, H. Weissig, I. N. Shindyalov, P. E. Bourne, *Nucleic Acids Res.* **2000**, *28*, 235–242.
[33] K. Hoffmann, G. Brosch, P. Loidl, M. Jung, *Nucleic Acids Res.* **1999**, *27*, 2057–2058.
[34] B. Heltweg, F. Dequiedt, E. Verdin, M. Jung, *Anal. Biochem.* **2003**, *319*, 42–48.
[35] K. Schmidt, R. Gust, M. Jung, *Arch. Pharm.* **1999**, *332*, 353–357.
[36] F. Zymalkowski, *Arch. Pharm.* **1958**, *291*, 436–442.
[37] Tripos Inc., St. Louis, MO (USA) **2005**.

Received: June 27, 2008
Revised: November 4, 2008
Published online on December 17, 2008

